Communication

Generation of Flat Terahertz Noise by Mixing Incoherent Light Fields

Youwen Zhang [1], Wenjie Liu [2], Ya Guo [3], Junbin Liu [2], Zhiwei Jia [1,*], Yuehui Sun [2], Anbang Wang [1,2] and Yuncai Wang [2,*]

[1] Key Laboratory of Advanced Transducers and Intelligent Control System, Ministry of Education and Shanxi Province, College of Electronic Information and Optical Engineering, Taiyuan University of Technology, Taiyuan 030024, China; zhangyouwen1249@link.tyut.edu.cn (Y.Z.); abwang@gdut.edu.cn (A.W.)

[2] Key Laboratory of Photonics Technology for Integrated Sensing and Communication, Guangdong University of Technology, Ministry of Education, Guangzhou 510006, China; wjliu@gdut.edu.cn (W.L.); 2112015079@mail2.gdut.edu.cn (J.L.); yhsun@gdut.edu.cn (Y.S.)

[3] School of Electronics and Information, Northwestern Polytechnical University, Xi'an 710072, China; 816guoya@mail.nwpu.edu.cn

[*] Correspondence: jiazhiwei@tyut.edu.cn (Z.J.); wangyc@gdut.edu.cn (Y.W.)

Abstract: Terahertz (THz) noise sources play an irreplaceable role in testing THz devices and evaluating THz application systems, and the flatness of their radio frequency (RF) spectra is an important technical parameter. In this paper, a scheme for generating flat THz noise by mixing multiple filtered incoherent light fields is proposed. A theoretical analysis is conducted to investigate the impact of different spectral linewidths and central wavelength differences of incoherent light fields on the noise power and RF spectrum flatness, and an optimized experimental scheme is obtained. The results show that the proposed method can generate a 280–380 GHz flat THz noise signal with an RF spectrum flatness of ±0.5 dB in simulation and ±2.7 dB in our experiments. This article provides an excellent technical solution to the demand for flat THz noise in the THz field.

Keywords: optical devices; flatness; incoherent light; opto-electrical conversion; terahertz noise

1. Introduction

Terahertz (THz) waves refer to electromagnetic waves with frequencies ranging from 0.1 to 10 THz [1], and have significant applications in various fields such as communication systems [2–5], radar imaging [6–10], sensing technology [11–14], metamaterial absorbers [15–17], and military equipment [18,19]. THz noise sources are an essential measurement tool for radar performance testing and receiver demodulation threshold detection [20,21]. In addition, THz noise sources can be widely used to characterize THz components and devices [22,23], evaluate a THz system's dynamic range and sensitivity [24], analyze gas composition [25], and perform incoherent imaging [26]. Recently, an increasing number of single-frequency THz devices and application systems have been developed and many of them are operating in the 300 GHz band according to the demands of communication and radar [27,28]. For example, Yi et al. reported a photonic source based on stimulated Brillouin scattering for 300 GHz wireless communication [29]. Seo et al. reported fundamental fixed-frequency and voltage-controlled oscillators operating at 346 GHz [30]. Consequently, noise sources in the corresponding frequency band are urgently needed to characterize relevant devices. The noise radio frequency (RF) spectrum flatness is of significant importance, and a flat RF power spectrum distribution can enhance the application of a noise source. For instance, in the measurement of a system with a large dynamic range, the noise with a flat RF spectrum can improve the dynamic accuracy and eliminate the need for tedious calibrations [31].

The existing technical solutions for generating THz noise sources include thermal [32,33], electronic [34,35], and photonic methods [36,37]. Thermal noise sources can generate

THz noise with a flat RF spectrum. However, they require low-temperature operating environments, have large volumes, and generate noise with low output power [38]. The electronic method involves utilizing electronic components such as Schottky diodes and transistors to directly generate THz noise. Goncalves et al. generated a 130–170 GHz integrated noise source based on an avalanche silicon Schottky diode in BiCMOS 55 nm [39]. Ehsan et al. used a GaAs Schottky diode to generate a 160–210 GHz noise signal [40]. However, owing to limitations in the operating bandwidth of electronic devices, the output power of electronic noise sources drops to a negligible and unsuitable level in the THz band.

Photonic technology, which breaks the bandwidth bottleneck, is a suitable alternative for generating THz noise. The most direct scheme is the conversion of broadband optical amplifier spontaneous emission (ASE) to a noise signal by using an optical-to-electrical (O-E) converter [41]. However, the noise power is low and the noise RF spectrum is not flat because the optical power is dispersed over a broad frequency band. Song et al. proposed a method for 280–380 GHz noise generation by mixing two wavelength-sliced ASE light fields using a uni-traveling carrier photodiode (UTC-PD), which can significantly improve noise power [42]. However, the noise RF spectrum was very narrow and not flat. In order to cover the frequency range of 280–380 GHz, it is necessary to change the filtering frequency bands multiple times. In our previous work, we proposed and demonstrated a scheme that mixes three incoherent light fields, through which the noise power and bandwidth can be easily controlled and the flatness of the noise RF spectrum can be optimized. A 20–50 GHz noise signal and a 130–170 GHz noise signal were generated [43,44].

In this study, we propose a scheme to generate a THz noise signal in the 280–380 GHz frequency band by mixing seven filtered incoherent light fields. Compared to the previous approach, different numbers of incoherent light fields and theoretical model are used, and the impact of the relative noise power is considered. A theoretical analysis is conducted to investigate the impact of different spectral linewidths and central wavelength differences on the noise power and RF spectrum flatness, and an optimized experimental scheme is obtained. The results indicate that the experiment can generate a 280–380 GHz flat THz noise with an RF spectrum flatness of only ± 2.7 dB. Compared with previous noise generation methods, our proposed method has a significant advantage in achieving a noise signal with a broadband and flat RF spectrum. Further work will consider the use of this noise source to characterize the receiver operating at 280–380 GHz to improve the dynamic accuracy and measurement efficiency.

2. Theoretical Principle

First, we simulated the generation of THz noise by mixing incoherent light fields to optimize the scheme for the target band of 280–380 GHz. Incoherent light fields can be converted to electrical noise using an O-E converter based on the square-law characteristic [45]. Given the Gaussian-shaped spectrum incoherent light fields, the RF spectrum of the generated electrical noise signal, $s_a(f)$, can be described as [46,47]

$$S_a(f) = \frac{2kR_0\Re^2(f)P^2}{m\sqrt{\pi}\Lambda}\left\{\frac{1}{m}\exp\left\{-\frac{[f-(\nu_m-\nu_{m-1})]^2}{4\Lambda^2}\right\} + \ldots + \frac{1}{m}\exp\left\{-\frac{[f-(\nu_m-\nu_1)]^2}{4\Lambda^2}\right\} + \exp\left(-\frac{f^2}{4\Lambda^2}\right)\right\} \tag{1}$$

where m is the number of wavelength-sliced incoherent light fields, v_m represents the m-th central frequency, Λ represents the spectral full-width at half maximum (FWHM) of incoherent light fields, k represents the maximum power transfer, R_0 is the system impedance, $\Re(f)$ is the responsivity of the frequency characteristics of the O-E converter, and P represents the average optical power. Here, we define the RF spectrum flatness as the difference between the maximum and minimum values of the RF spectrum in the target band 280–380 GHz.

Figure 1 shows the simulation results of THz noise generation achieved by employing different incoherent light field mixing schemes based on Equation (1). Converted from an incoherent light field with a spectral width of 46 nm, as shown in Figure 1a, the noise RF

spectrum covers a wide frequency range. The output electrical noise power decreases with an increase in the frequency. Consequently, a very large part of the noise energy is outside of the target band, leading to low noise power. In addition, the RF spectrum flatness is ±2.4 dB.
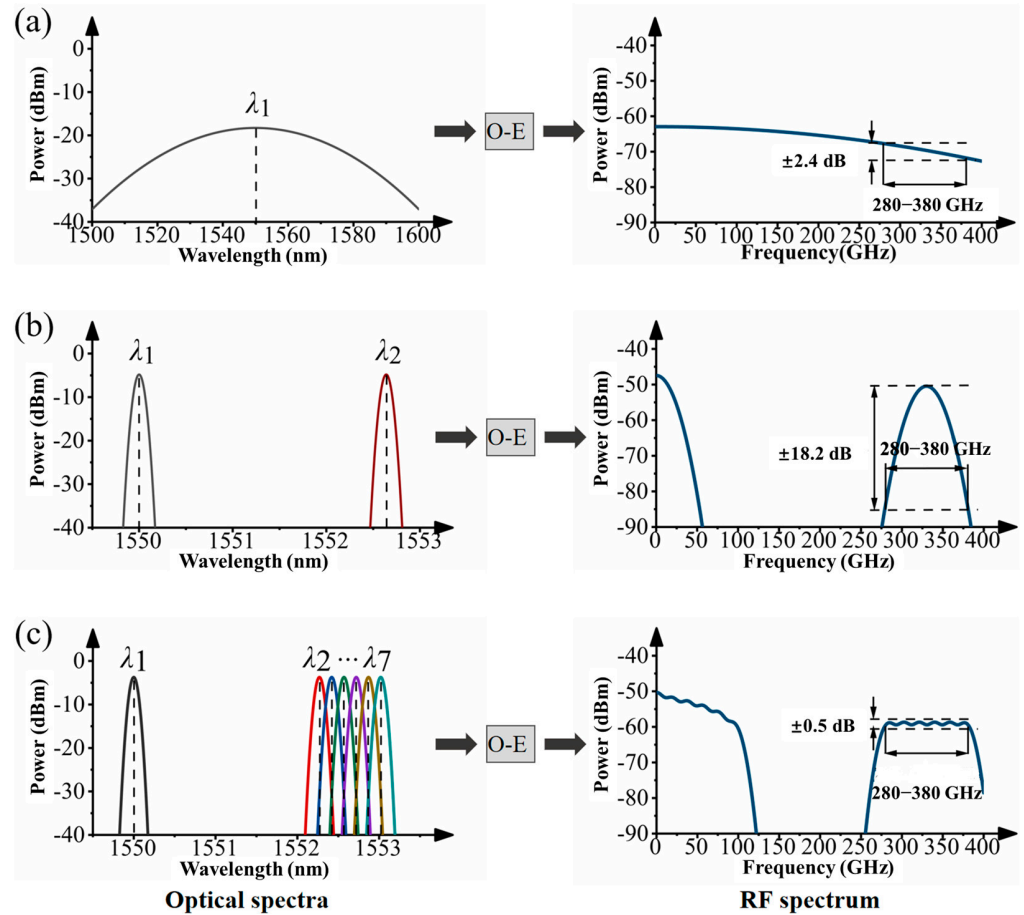

Figure 1. Simulation results of optical spectra and RF spectra of noise generation by incoherent light fields: (**a**) incoherent light field without filtering; (**b**) two filtered incoherent light fields mixing; (**c**) multiple filtered incoherent light fields mixing. λ, the central wavelength of the optical spectra.

Figure 1b illustrates the simulation results for the modified scheme of noise generation obtained by mixing two incoherent light fields. Two incoherent light fields with an FWHM value of 0.1 nm are obtained after filtering. The center frequency of the noise RF spectrum depends on the difference between the two central wavelengths and is given as

$$f = c/\lambda_1 - c/\lambda_2, \tag{2}$$

where c represents the speed of light. According to the calculation results, the central wavelengths are λ_1 = 1550.00 nm and λ_2 = 1552.64 nm, and the center frequency is f = 330.0 GHz. The simulated RF spectrum shows that most of the electrical noise power can be centered on the center frequency, and the power level is higher than that of an incoherent light field without filtering. However, because the optical spectra are narrow, the RF spectrum is not flat, and the RF spectrum flatness is ±18.2 dB.

Furthermore, a method involving the mixing of multiple incoherent light fields can be used to generate a broadband noise signal with a flat RF spectrum, as shown in Figure 1c. In this manner, the incoherent source is filtered into several light fields with different central wavelengths, and the FWHM of each light field is 0.1 nm. After the calculation, seven filtered light fields are obtained, and the central wavelengths are λ_1 = 1550.00 nm,

λ_2 = 1552.27 nm, λ_3 = 1552.42 nm, λ_4 = 1552.57 nm, λ_5 = 1552.72 nm, λ_6 = 1552.87 nm, and λ_7 = 1553.02 nm. The central wavelength difference between each pair of incoherent light fields (i.e., $\lambda_1 - \lambda_2$, $\lambda_1 - \lambda_3$, $\lambda_1 - \lambda_4$, ... , and $\lambda_1 - \lambda_7$) determines the corresponding center frequency of the RF spectrum. The beating of the incoherent light field centered at λ_1 and the other light fields (λ_2, ... λ_6, and λ_7) generates electrical noise with six different center frequencies, resulting in a broadband flat RF spectrum in the 280–380 GHz range, and the RF spectrum flatness is as low as ±0.5 dB. Notably, the incoherent light fields centered at λ_2, ... λ_6, and λ_7 will also beat each other and generate noise signals. Nevertheless, these noise signals cover the low-frequency band because the differences between their wavelengths are small, and their frequencies are not in the target frequency band. According to this principle and Equation (1), by adjusting the number and central wavelengths of the filtered incoherent light fields, we can generate electrical noise in any desired frequency range.

To optimize the power and RF spectrum flatness of THz noise generated by seven incoherent light fields mixing, numerical simulation is conducted to investigate the impact of different FWHM values and central wavelength differences on the relative noise power and RF spectrum flatness in the target frequency range. Here, we define the relative power as the ratio of noise power within the target frequency range of 280–380 GHz to the noise power outside the target frequency range. Figure 2a shows the variation in relative noise power as the FWHM value and the difference in central wavelengths among the last six incoherent light fields are changed while keeping the output optical power constant. The simulation results indicate that as the difference in central wavelengths among the last six incoherent light fields increases, the relative power of the noise decreases. Additionally, when the central wavelength difference is within the range of 0.1–0.25 nm, the relative power decreases as the FWHM value increases. However, when the central wavelength difference reaches 0.3 nm, the relative power increases with an increase in the FWHM value. Figure 2b depicts the simulation results for the variation in the RF spectrum flatness of the 280–380 GHz noise. Except for the central wavelength differences of 0.1–0.15 nm, the RF spectrum flatness generally decreases as the FWHM value increases for other central wavelength differences. Considering both the impact of the relative power and the RF spectrum flatness, we chose the incoherent light field with a central wavelength difference of 0.15 nm and an FWHM of 0.1 nm for further experiments. The theoretical relative power in this case is 0.40, and the RF spectrum flatness is 1 dB, which corresponds to ±0.5 dB.
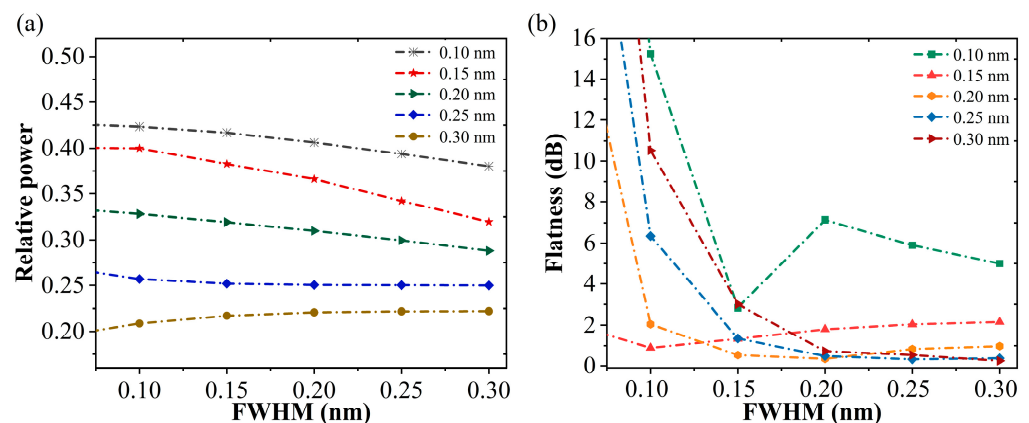

Figure 2. Simulation results of relative power and RF spectrum flatness: (**a**) relative power; (**b**) RF spectrum flatness.

3. Results and Discussion

3.1. Experimental Setup

The experimental setup of the proposed method is shown in Figure 3. First, the incoherent light field generated using the super-luminescent diode (SLD) is decoupled into multiple channels by an optical coupler (OC). Then, multiple optical tunable filters (OTFs)

with different central wavelengths are used to filter and shape each channel to obtain multiple Gaussian-shaped spectral light fields with the same FWHM value of 0.1 nm. These filtered light fields are coupled using another OC and amplified using an erbium-doped fiber amplifier (EDFA) to ensure that the output optical power is maintained at 15 dBm. The UTC-PD operating in the frequency range of 280–380 GHz with a DC conversion efficiency of 0.22 A/W (NTT Electronics Corp. IOD-PMJ-13001) [48] then converts the optical noise signal to the electrical domain. To measure the RF spectrum using an electronic spectrum analyzer (ESA), the electrical noise signal from the UTC-PD is down-converted with a diode harmonic mixer. Notably, the ESA used in this experiment is equipped with the B21 module (local-oscillator (LO)/intermediate-frequency (IF) connection for external mixer), and we can measure the THz signals without external LO signals.
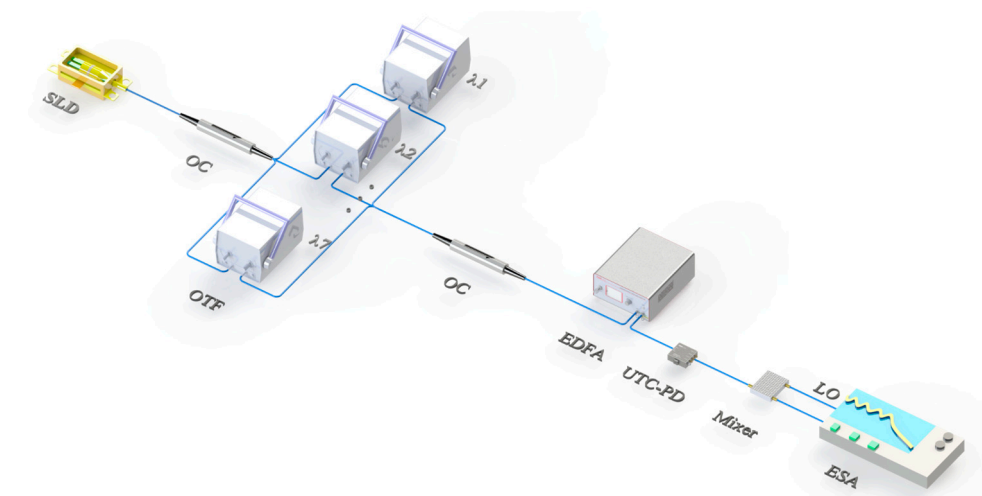

Figure 3. Experimental setup of THz noise generation. SLD, superluminescent diode; OTF, optical tunable filter; OC, optical coupler; EDFA, erbium-doped fiber amplifier; UTC-PD, uni-traveling carrier photodiode; LO, local oscillator; ESA, electrical spectrum analyzer.

3.2. Experimental Results and Analysis

Figure 4 displays the associated experimental results of the optical and RF spectra. First, we generated a noise signal using the SLD without separating into different channels and filtering for comparison. The optical spectrum is shown in Figure 4a. The central wavelength λ_1 was 1550.00 nm, and the entire optical spectrum from the SLD was sent to the UTC-PD. To eliminate the impact of the optical power difference, the optical power output into the UTC-PD was maintained at 15 dBm, similar to subsequent incoherent light field mixing schemes. Figure 4b depicts the associated experimental RF spectrum. The output electrical noise power decreased with an increase in the frequency, and the RF spectrum flatness was ± 5.6 dB in the 280–380 GHz range. The differences between simulation results and experimental results can be attributed to the non-flat response curve of the UTC-PD and the impact of the internal system noise from the mixer and amplifier.

The noise signal could also be generated by mixing two filtered incoherent light fields with the central wavelengths of λ_1 = 1550.00 nm and λ_2 = 1552.64 nm, and the FWHM value of the optical spectra was 0.1 nm (Figure 4c). An uneven noise RF spectrum was produced. Figure 4d shows the experimental result obtained using this scheme, and the resulting RF spectrum flatness was ± 14.4 dB. As the optical power was identical to that in the aforementioned no-filtering method, the output noise power in this method could center on the frequency of f = 330.0 GHz; however, it attenuated rapidly in higher or lower frequencies, leading to a poor RF spectrum flatness over the frequency range of 280–380 GHz.
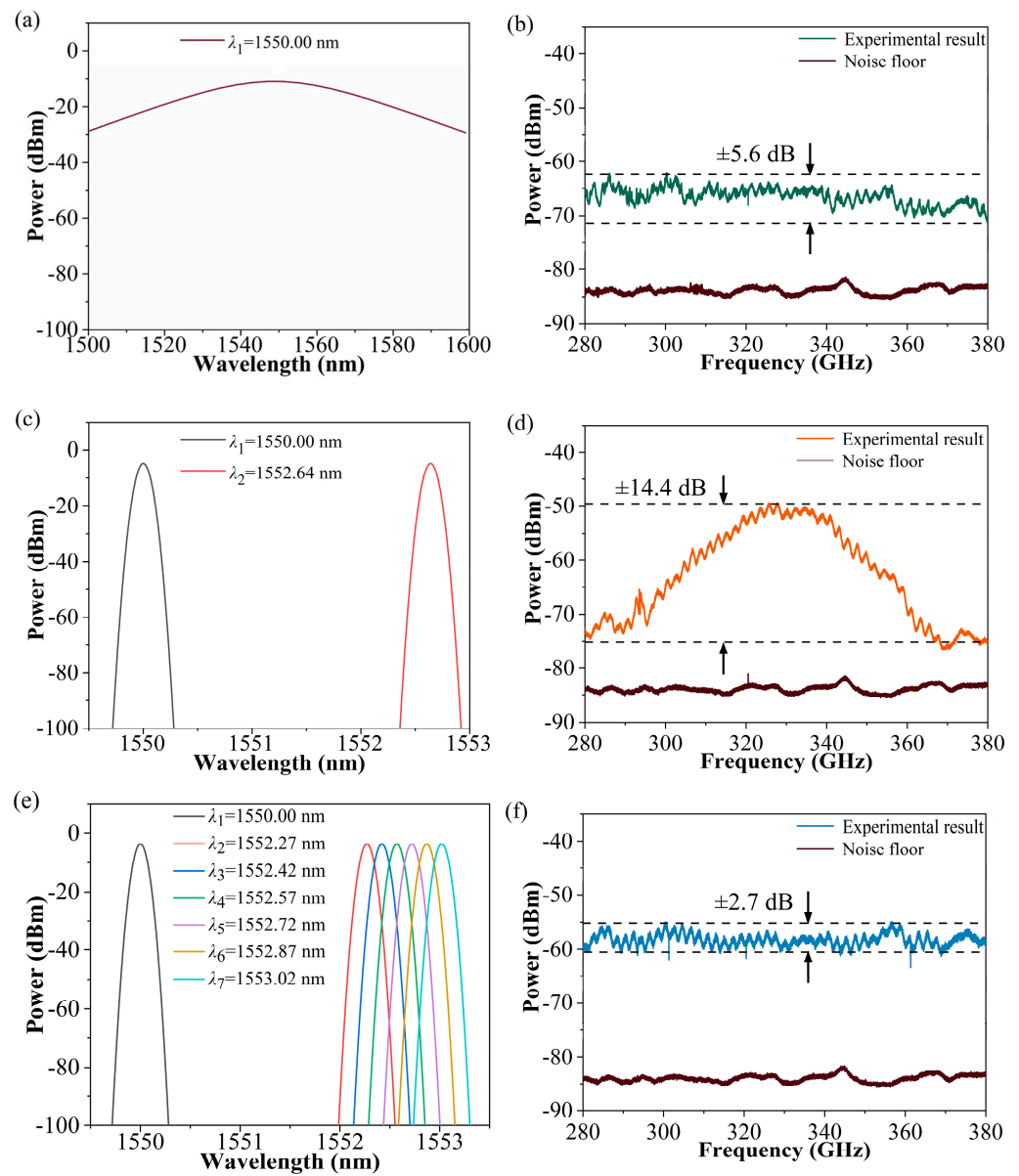
Figure 4. Experimental results of optical spectra and RF spectra. Experimental optical spectra: (**a**) incoherent light field source without separating and filtering; (**c**) two incoherent light fields mixing; (**e**) seven incoherent light fields mixing. Experimental RF spectrum: (**b**) incoherent light field source without separating and filtering; (**d**) two incoherent light fields mixing; (**f**) seven incoherent light fields mixing.

Furthermore, the noise signal was generated by mixing seven incoherent light fields. Based on the proposed principle, seven optical spectra with different central wavelengths can be generated, as shown in Figure 4e. Similar to the simulation, the corresponding calculated central wavelengths were $\lambda_1 = 1550.00$ nm, $\lambda_2 = 1552.27$ nm, $\lambda_3 = 1552.42$ nm, $\lambda_4 = 1552.57$ nm, $\lambda_5 = 1552.72$ nm, $\lambda_6 = 1552.87$ nm, and $\lambda_7 = 1553.02$ nm. The optical power launching into the UTC-PD was identical to 15 dBm in the three approaches, and the FWHM value of the optical spectra was 0.1 nm. The beats between the filtered incoherent light field centered at λ_1, and the other six filtered incoherent lights produced six different center frequencies in the RF spectrum. Figure 4f presents the experimental result of the RF spectrum. The spacings between the center frequencies were designed to be identical, and the center frequencies were $f_1 = 283.75$ GHz, $f_2 = 302.50$ GHz, $f_3 = 321.25$ GHz, $f_4 = 340.00$ GHz, $f_5 = 358.75$ GHz, and $f_6 = 377.50$ GHz. Therefore, after the superposition

of these frequencies, a flat RF spectrum ranging 280–380 GHz could be achieved, and the corresponding RF spectrum flatness in the experimental result was as low as ±2.7 dB. In terms of the previously mentioned influencing factors, the experimental results agreed well with the simulation results. The comparison of these three sets of experimental results clarifies that seven filtered incoherent light fields can be mixed to optimize the RF spectrum flatness by more than ±2.9 dB in the 280–380 GHz range compared with the scheme of using incoherent light fields without filtering and more than ±11.7 dB compared with the mixing of two filtered incoherent light fields. Moreover, the entire SLD optical spectrum without filtering has an excessively broad bandwidth, and only part of it can be converted to the noise signal in our target frequency band. The electrical noise power level of the seven incoherent light fields scheme is higher than that of the scheme without filtering in the 280–380 GHz range. Table 1 lists the flatness and bandwidth of the THz noise sources reported in recent years.

Table 1. Flatness and bandwidth of noise sources in comparison to this work.

Flatness (dB)	Bandwidth (GHz)	Frequency Range (GHz)	Ref
±2	40	130–170	[39]
±3	30	170–200	[40]
±3.5	110	125–235	[35]
±2.5	15	290–305	[42]
±2.5	60	260–320	[41]
±2.7	100	280–380	This work

4. Conclusions

In this study, we have proposed and demonstrated a broadband THz noise generation technique that involves mixing multiple incoherent light fields. A theoretical analysis has been conducted to investigate the impact of different spectral linewidths and central wavelength differences of incoherent light fields on the noise power and RF spectrum flatness. The results obtained show that the proposed method can generate a 280–380 GHz noise signal with an RF spectrum flatness of ±2.7 dB. Compared with the existing noise generation methods, our method has a significant advantage in achieving a broadband and flat RF spectrum. It can characterize 280–380 GHz components and devices such as receivers and amplifiers without tedious calibrations. Moreover, based on our theoretical principle, the central wavelengths of the filtered incoherent light fields can be precisely adjusted to generate a noise signal in different high-frequency bands depending on the demand. We believe that this noise generation method will play a significant role in THz applications in the future.

Author Contributions: Conceptualization, Y.Z., Y.G. and J.L.; methodology, Y.Z., W.L., Z.J. and Y.W.; simulation, Y.Z. and J.L.; validation, Y.Z., Y.G. and J.L.; writing—original draft preparation, Y.Z. and W.L.; writing—review and editing, Z.J., Y.S., A.W. and Y.W.; project administration, Y.W.; funding acquisition, A.W. and Y.W. All authors have read and agreed to the published version of the manuscript.

Institutional Review Board Statement: Not applicable.

Informed Consent Statement: Not applicable.

Data Availability Statement: No new or additional data are available.

Conflicts of Interest: The authors declare no conflict of interest.

References

1. Han, C.; Chen, Y. Propagation modeling for wireless communications in the terahertz band. *IEEE Commun. Mag.* **2018**, *56*, 96–101. [CrossRef]
2. Minoru, F. Overview of sub-terahertz communication and 300 GHz CMOS transceivers. *IEICE Electron. Express* **2021**, *18*, 2002.
3. Nagatsuma, T.; Ducournau, G.; Renaud, C.C. Advances in terahertz communications accelerated by photonics. *Nat. Photonics* **2016**, *10*, 371–379. [CrossRef]
4. Gonzalez-Guerrero, L.; Shams, H.; Fatadin, I.; Fice, M.J.; Naftaly, M.; Seeds, A.J.; Renaud, C.C. Comparison of Optical Single Sideband Techniques for THz-Over-Fiber Systems. *IEEE Trans. Terahertz Sci. Technol.* **2019**, *9*, 98–105. [CrossRef]
5. Song, H.J.; Lee, N. Terahertz communications: Challenges in the next decade. *IEEE Trans. Terahertz Sci. Technol.* **2021**, *12*, 105–117. [CrossRef]
6. Božanić, M.; Sinha, S. Emerging transistor technologies capable of terahertz amplification: A way to re-engineer terahertz radar sensors. *Sensors* **2019**, *19*, 2454. [CrossRef] [PubMed]
7. Zhang, X.; Chang, T.; Wang, Z.; Cui, H. Three-Dimensional Terahertz Continuous Wave Imaging Radar for Nondestructive Testing. *IEEE Access* **2020**, *8*, 144259–144276. [CrossRef]
8. Mittleman, D.M. Twenty years of terahertz imaging. *Opt. Express* **2018**, *26*, 9417–9431. [CrossRef]
9. Chi, T.; Huang, M.; Li, S.; Wang, H. A packaged 90-to-300 GHz transmitter and 115-to-325 GHz coherent receiver in CMOS for full-band continuous-wave mm-wave hyperspectral imaging. In Proceedings of the IEEE International Solid-State Circuits Conference, San Francisco, CA, USA, 5 February 2017; p. 16724546.
10. Zhang, Z.; Qi, P.; Guo, L.; Zhang, N.; Lin, L.; Liu, W. Review on Super-Resolution Near-Field Terahertz Imaging Methods. *Acta Opt. Sin.* **2023**, *43*, 0600001.
11. Singh, R.; Cao, W.; Al-Naib, I.; Cong, L.; Withayachumnankul, W.; Zhang, W. Ultrasensitive terahertz sensing with high-Q Fano resonances in metasurfaces. *Appl. Phys. Lett.* **2014**, *105*, 171101. [CrossRef]
12. Naftaly, M.; Vieweg, N.; Deninger, A. Industrial applications of terahertz sensing: State of play. *Sensors* **2019**, *19*, 4203. [CrossRef]
13. Javadi, E.; But, D.B.; Ikamas, K.; Zdanevicius, J.; Knap, W.; Lisauskas, A. Sensitivity of Field-Effect Transistor-Based Terahertz Detectors. *Sensors* **2021**, *21*, 2909. [CrossRef]
14. Tonouchi, M. Cutting-edge terahertz technology. *Nat. Photonics* **2007**, *1*, 97–105. [CrossRef]
15. Xu, W.; Xie, L.; Ying, Y. Mechanisms and applications of terahertz metamaterial sensing: A review. *Nanoscale* **2017**, *9*, 13864–13878. [CrossRef] [PubMed]
16. Degl'Innocenti, R.; Lin, H.; Navarro-Cía, M. Recent progress in terahertz metamaterial modulators. *Nanophotonics* **2022**, *11*, 1485–1514. [CrossRef]
17. Wang, B.X.; Xu, C.; Duan, G.; Xu, W.; Pi, F. Review of broadband metamaterial absorbers: From principles, design strategies, and tunable properties to functional applications. *Adv. Funct. Mater.* **2023**, *33*, 2213818. [CrossRef]
18. Zhang, J.; Yang, Y. Military Application of Terahertz Technology in the Future Ground-Air Integrative Battlefield. *Ship Electron. Eng.* **2020**, *40*, 9–11.
19. Strag, M.; Świderski, W. Non-destructive inspection of military-designated composite materials with the use of Terahertz imaging. *Compos. Struct.* **2023**, *306*, 116588. [CrossRef]
20. Orlando, D. A novel noise jamming detection algorithm for radar applications. *IEEE Signal Process Lett.* **2016**, *24*, 206–210. [CrossRef]
21. Li, D.; Minoia, G.; Repossi, M.; Baldi, D.; Temporiti, E.; Mazzanti, A.; Svelto, F. A low-noise design technique for high-speed CMOS optical receivers. *IEEE J. Solid-State Circuits* **2014**, *49*, 1437–1447. [CrossRef]
22. Hsiao, H.F.; Tu, C.H.; Chang, D.C.; Juang, Y.Z. Noise figure verification using cold-source and Y-factor technique for amplifier and down-converted mixer. In Proceedings of the Asia-Pacific Microwave Conference, Sendai, Japan, 4 November 2014; pp. 901–903.
23. Ahmed, A.R.; Lee, D.H.; Yeom, K.W. On-wafer noise parameters measurement using an extended six-port network and conventional noise figure analyzer. *Int. J. Microw. Wirel. Technol.* **2017**, *9*, 821–829. [CrossRef]
24. Shahriar, C.; Pan, M.L.; Lichtman, M.; Clancy, T.C.; McGwier, R.; Tandon, R.; Sodagari, S.; Reed, J.H. PHY-layer resiliency in OFDM communications: A tutorial. *Int. J. Microw. Wirel. Technol.* **2014**, *17*, 292–314. [CrossRef]
25. Song, H.J.; Shimizu, N.; Furuta, T.; Wakatsuki, A.; Nagatuma, T. Photonic generation of sub-terahertz noises and its application to spectroscopy measurement. In Proceedings of the 38th European Microwave Conference, Amsterdam, The Netherlands, 27 October 2008; p. 10414969.
26. Nagatsuma, T.; Kumashiro, T.; Fujimoto, Y.; Taniguchi, K.; Ajito, K.; Kukutsu, N.; Furuta, T.; Wakatsuki, A.; Kado, Y. Millimeter-wave imaging using photonics-based noise source. In Proceedings of the 34th International Conference on Infrared, Millimeter, and Terahertz Waves, Busan, Republic of Korea, 21 September 2009; p. 10976884.
27. Fujishima, M. Future of 300 GHz band wireless communications and their enabler, CMOS transceiver technologies. *Jpn. J. Appl. Phys.* **2021**, *60*, SB0803. [CrossRef]
28. Rubio-Cidre, G.; Badolato, A.; Ubeda-Medina, L.; Grajal, J.; Mencia-Oliva, B.; Dorta-Naranjo, B. DDS-based signal-generation architecture comparison for an imaging radar at 300 GHz. *IEEE Trans. Instrum. Meas.* **2015**, *64*, 3085–3098. [CrossRef]
29. Yi, L.; Iwamoto, K.; Yamamoto, T.; Ayano, F.; Rolland, A.; Kuse, N.; Fermann, M.; Li, Y.; Nagatsuma, T. 300-GHz-band wireless communication using a low phase noise photonic source. *Int. J. Microw. Wirel. Technol.* **2020**, *12*, 551–558. [CrossRef]

30. Seo, M.; Urteaga, M.; Young, A.; Jain, V.; Griffith, Z.; Hacker, J.; Rowell, P.; Pierson, R.; Rodwell, M. >300GHz fixed-frequency and voltage-controlled fundamental oscillators in an InP DHBT process. In Proceedings of the IEEE MTT-S International Microwave Symposium, Anaheim, CA, USA, 23 May 2021; pp. 272–275.

31. Pepe, D.; Barnett, C.; D'Amore, G.; Zito, D. On-chip millimeter-wave cold-source noise figure measurements with PNA-X. *IEEE Trans. Instrum. Meas.* **2017**, *66*, 3399–3401. [CrossRef]

32. Chen, C.H.; Wang, Y.L.; Bakr, M.H.; Zeng, Z. Novel noise parameter determination for on-wafer microwave noise measurements. *IEEE Trans. Instrum. Meas.* **2008**, *57*, 2462–2471. [CrossRef]

33. Tiemeijer, L.F.; Havens, R.J.; Kort, R.; Scholten, A.J. Improved Y-factor method for wide-band on-wafer noise-parameter measurements. *IEEE Trans. Microw. Theory Tech.* **2005**, *53*, 2917–2925. [CrossRef]

34. Arslan, S.; Yıldırım, B.S. A broadband microwave noise generator using zener diodes and a new technique for generating white noise. *IEEE Microw. Wirel. Compon. Lett.* **2018**, *28*, 329–331. [CrossRef]

35. Forstén, H.; Saijets, J.H.; Kantanen, M.; Varonen, M.; Kaynak, M.; Piironen, P. Millimeter-wave amplifier-based noise sources in SiGe BiCMOS technology. *IEEE Trans. Microw. Theory Tech.* **2021**, *69*, 4689–4696. [CrossRef]

36. Song, H.J.; Yaita, M. On-wafer noise measurement at 300 GHz using UTC-PD as noise source. *IEEE Microw. Wirel. Compon. Lett.* **2014**, *24*, 578–580. [CrossRef]

37. Ustinov, A.B.; Kondrashov, A.V.; Kalinikos, B.A. A microwave photonic generator of chaotic and noise signals. *Tech. Phys. Lett.* **2016**, *42*, 403–406. [CrossRef]

38. Beland, P.; Labonte, S.; Roy, L.; Stubbs, M. A novel on-wafer resistive noise source. *IEEE Microw. Guided Wave Lett.* **1999**, *9*, 227–229. [CrossRef]

39. Goncalves, J.C.A.; Quemerais, T.; Gloria, D.; Avenier, G.; Lepilliet, S.; Ducournau, G.; Gaquière, C.; Danneville, F. A 130 to 170 GHz integrated noise source based on avalanche silicon Schottky diode in BiCMOS 55 nm for in-situ noise characterization. In Proceedings of the International Conference of Microelectronic Test Structures, Grenoble, France, 27 March 2017; p. 16970484.

40. Ehsan, N.; Piepmeier, J.; Solly, M.; Macmurphy, S.; Lucey, J.; Wollack, E. A robust waveguide millimeter-wave noise source. In Proceedings of the European Microwave Conference, Paris, France, 7 September 2015; p. 15649195.

41. Ghanem, H.; Lépilliet, S.; Danneville, F.; Ducournau, G. 300-GHz intermodulation/noise characterization enabled by a single THz photonics source. *IEEE Microw. Wirel. Compon. Lett.* **2020**, *30*, 1013–1016. [CrossRef]

42. Song, H.J.; Shimizu, N.; Kukutsu, N.; Nagatsuma, T.; Kado, Y. Microwave photonic noise source from microwave to sub-terahertz wave bands and its applications to noise characterization. *IEEE Trans. Microw. Theory Tech.* **2008**, *56*, 2989–2997. [CrossRef]

43. Sun, Y.; Guo, Y.; Wang, Y.; Liu, W.; Huang, H.; Huang, Y.; Qin, Y. Generation of 130–170 GHz flat millimeter-wave noise signal. *Sci. Sin. Inform.* **2022**, *52*, 2155–2162.

44. Sun, Y.; Chen, Y.; Li, P.; Zinsou, R.; Wang, A.; Wang, Y. Flat Millimeter-Wave Noise Generation by Optically Mixing Multiple Wavelength-Sliced ASE Lights. *IEEE Photonics Technol. Lett.* **2021**, *33*, 1270–1273. [CrossRef]

45. Vidal, B. Broadband photonic microwave noise sources. *IEEE Photonics Technol. Lett.* **2020**, *32*, 592–594. [CrossRef]

46. Derickson, D. *Fiber Optic Test and Measurement*, 3rd ed.; Prentice-Hall: Englewood Cliffs, NJ, USA, 1998; pp. 169–220.

47. Nzarathy, M.; Sorin, W.V.; Baney, D.M.; Newton, S.A. Spectral analysis of optical mixing measurements. *J. Light. Technol.* **1989**, *7*, 1083–1096.

48. Ishibashi, T.; Muramoto, Y.; Yoshimatsu, T.; Ito, H. Unitraveling-carrier photodiodes for terahertz applications. *IEEE J. Sel. Top. Quantum Electron.* **2014**, *20*, 79–88. [CrossRef]